A photon-counting detector for exoplanet missions*

D. F. Figer[†a], J. Lee[a], B. J. Hanold[a], B. F. Aull[b], J. A. Gregory[b], D. R. Schuette[b]
[a]Center for Detectors, Rochester Institute of Technology,
74 Lomb Memorial Drive, Rochester, NY 14623;
[b]Lincoln Laboratory, Massachusetts Institute of Technology,
244 Wood St, Lexington, MA 02420

ABSTRACT

This paper summarizes progress of a project to develop and advance the maturity of photon-counting detectors for NASA exoplanet missions. The project, funded by NASA ROSES TDEM program, uses a 256×256 pixel silicon Geiger-mode avalanche photodiode (GM-APD) array, bump-bonded to a silicon readout circuit. Each pixel independently registers the arrival of a photon and can be reset and ready for another photon within 100 ns. The pixel has built-in circuitry for counting photo-generated events. The readout circuit is multiplexed to read out the photon arrival events. The signal chain is inherently digital, allowing for noiseless transmission over long distances. The detector always operates in photon counting mode and is thus not susceptible to excess noise factor that afflicts other technologies. The architecture should be able to operate with shot-noise-limited performance up to extremely high flux levels, $>10^6$ photons/second/pixel, and deliver maximum signal-to-noise ratios on the order of thousands for higher fluxes. Its performance is expected to be maintained at a high level throughout mission lifetime in the presence of the expected radiation dose.

Keywords: detector, read noise, avalanche photodiode, array, exoplanet

1. INTRODUCTION

NASA's ultimate goal in exploring extrasolar planets (exoplanets) is to identify bodies like Earth that can support life. Exoplanet missions have been in development for the past fifteen years, and the first such dedicated space mission, *Kepler*, is now collecting data. *NASA* anticipates operating a series of future exoplanet missions having progressively greater sensitivity for detecting and characterizing gas giant and Earth-like planets [1]. So far, exoplanets have rarely been detected by direct imaging, but some future exoplanet missions plan to use this technique to image Earth-like planets orbiting nearby stars. This plan relies heavily on a broad program of technology development, including low noise detectors that deliver the highest possible sensitivity for detecting faint objects.

Exoplanet spectroscopy depends critically on very low noise detectors because the weak light from the source is dispersed across many pixels. Photon-counting avalanche photodiode detectors promise zero read noise, high radiation hardness, low power, low mass, extreme linearity, and high dynamic range. This technology is currently at TRL 3. *NASA* chose Rochester Institute of Technology and MIT Lincoln Laboratory to advance a zero read noise imaging detector for this purpose through a radiation testing program. The detector is a 256×256 Geiger-mode avalanche photodiode (GM-APD) focal plane array that provides zero read noise, ultra-high dynamic range, and highly linear response over the relevant flux range of interest. It would be useful for a planet finding spectrograph, as a wavefront sensor, and for an imager.

The objectives of this project are to advance photon-counting detectors for *NASA* exoplanet missions from TRL 3 to TRL 5. Longer term, we anticipate development to TRL 6 with relatively little incremental effort and schedule time; validation at this level will include demonstration in a relevant testbed. The TPF-C Flight Baseline Mission Concept [2] defines system characteristics that we consider general enough for developing detectors in future exoplanet missions. Table 1 summarizes the most relevant system parameters. There will likely be a number of focal planes in an exoplanet

* The MIT Lincoln Laboratory portion of this work was performed under a Collaboration Agreement between MIT Lincoln Laboratory and Rochester Institute of Technology. Opinions, interpretations, conclusions, and recommendations are those of the authors, and do not necessarily represent the view of the United States Government.
† figer@cfd.rit.edu; phone 1 585 475-6005; fax 1 585 475-4250; http://ridl.cfd.rit.edu

mission. For example, in the case of TPF-C, various instrument concept studies require focal planes for a coronagraph, spectrograph, wavefront sensor, and wide-field general astrophysics camera. Several of these instruments could use a photon-counting detector.

Table 1. Exoplanet Mission Parameters

Parameter	*Specification*
Telescope Parameters	
Telescope Aperture Size	8 x 3.5 m
Effective Focal Length	140 m
Final f/#	f/18
Object and Background Parameters	
Star Brightness	5 mag
Planet Brightness	30 mag
Planet Brightness (imaging)	0.1 ph/s/pixel
Zodiacal Flux (imaging)	0.03 ph/s/pixel
Wavelength Coverage Parameters	
Wavelength Range	0.5-1.1 μm
Imaging Filter Resolution	5 (=λ/Δλ)
Spectroscopic Resolution	100 (=λ/Δλ)
Focal Plane Parameters	
Coronagraph Field Size	5 x 5 arcsec^2
Wide-field Camera Field Size	7 x 7 arcmin^2
Plate scale[b]	16 mas/pixel
Pixel size[b]	10 microns
Inner Working Angle	4λ/D=65 mas
Light Suppression Ratio	10^{-10}
Planet Brightness (spectroscopy)	0.006 ph/s/pixel

[a]The information in this table has been extracted or derived from the TPF-C Flight Baseline Mission Concept Report *[2]* and the TPF-C STDT Report *[3]*.[bc]The plate scale and pixel size are each halfway between what would be needed to critically sample the point spread functions along the short and long axes of the pupil.

2. EXOPLANET MISSION SENSITIVITY

A key challenge for an exoplanet mission is to detect a planet that contributes a very faint flux of about 0.2 photons/s (R=30 visual magnitude) distributed over a photometric aperture. For a critically sampled point spread function, this corresponds to a flux of about 0.1 photons/s/pixel in the central pixel. Spreading this flux across the focal plane of a spectrograph leads to even fainter fluxes. Assuming R~100 (=λ/Δλ), the resultant flux will be about 20 photons/hour/pixel. Potential noise sources for both spectroscopy and imaging are read noise, shot noise from the residual light from the star, shot noise from the zodiacal light, and shot noise from dark current.

With inherently zero readout noise, these devices will outperform existing ultra-low noise CMOS and CCD imagers in terms of noise, radiation immunity, power consumption, and mass. The equations in Figure 1 define two potentially useful metrics for exoplanet detection. "Detectivity" is one divided by the flux that generates a signal-to-noise ratio (SNR) of one; a larger detectivity indicates greater sensitivity. In the limit where read noise dominates, detectivity scales as one over the read noise. The second metric, "τ," is the exposure time required to generate a fixed SNR. Again, when read noise dominates, τ scales as the read noise. These metrics reflect the value of low detector read noise.

$$SNR = \frac{S}{N} = \frac{\eta_{inst} A \frac{\Delta\nu}{h\nu} F_\nu t QE_\nu}{\sqrt{\left(\eta_{inst} A \frac{\Delta\nu}{h\nu} F_\nu t QE_\nu\right) + \left(\eta_{inst} A \frac{\Delta\nu}{h\nu} F_{back,\nu} t QE_\nu\right) + i_{dark} t + N_{read}^2}}$$

$$\text{Sensitivity} \equiv N_{\gamma,SNR=1} = \text{flux at which SNR} = 1; \text{Detectivity} = \frac{1}{\text{sensitivity}} = \frac{1}{N_{\gamma,SNR=1}}.$$

$$\text{Detectivity} = \frac{2tQE}{1+\sqrt{1+4n_{pix}(N_{\gamma,background} tQE + i_{dark} t + N_{read}^2)}} \xrightarrow{\text{read noise dominated}} \frac{tQE}{N_{read}\sqrt{n_{pix}}}.$$

$$\tau = \text{exposure time to reach a particular SNR} \xrightarrow{SNR=1 \text{ and } N_{\gamma,background}=0 \text{ and } i_{dark}=0} \frac{N_{read}\sqrt{n_{pix}}}{N_\gamma QE}.$$

Figure 1. Detectivity and exposure time for read noise limited applications.

Consider a specific test case to dramatize the benefit of a photon-counting detector. Figure 2 (*left*) contains a table of exposure times needed to achieve SNR=1 per spectral element[‡] as a function of read noise and quantum efficiency for a 30th magnitude planet imaged in a spectrograph (R=100) with background contributions from zodiacal light and spillover from a nearby star, suppressed by 10^{10} using realizable nulling techniques [4]. The dark current is 0.001 e^-/second/pixel. The table shows that the observing time would be about a ***factor of two less*** with a photon-counting detector compared to a typical CCD. Figure 2 (*right*) is a graphic representation of the data in the table for QE=70%. While this spectroscopic case is most dramatic, the planet imaging detector and wavefront sensor would also benefit from photon-counting technology.

Exposure Time (seconds) for SNR = 1				
FOM		Quantum Efficiency		
		50%	70%	100%
read noise	0	680	453	300
	1	865	591	400
	2	1,209	841	577
	3	1,587	1,113	768
	4	1,976	1,392	964
	5	2,369	1,673	1,161
	6	2,764	1,956	1,359
	7	3,161	2,239	1,558
mag_star=5, mag_planet=30, R=100, i_dark=0.0010				

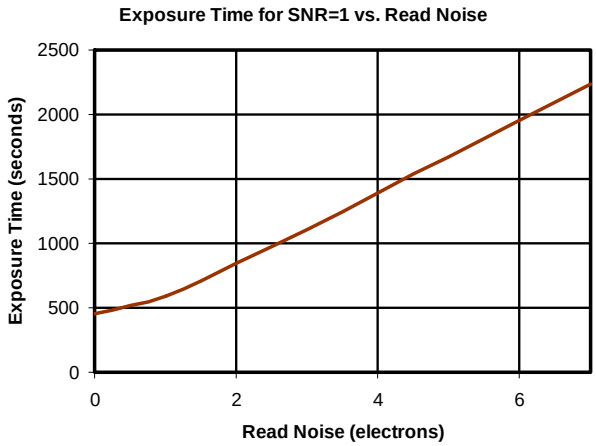

Figure 2. (left) A photon-counting detector (zero read noise) would deliver dramatic gains versus typical CCDs in system sensitivity and thus time to detect a planet. The table shows the time needed to reach SNR=1 versus read noise and quantum efficiency for a 30th magnitude planet imaged in a spectrograph (R=100) with background contributions from zodiacal light and spillover from a nearby star light, suppresed by 10^{10}. System parameters from Table 1 are assumed. The dark current is 0.001 electrons/second/pixel. (right) This is a plot of the data in the table for QE=70%.

3. PHOTON COUNTING DETECTOR FOR EXPLANET MISSIONS

Development of a photon counting imager will directly benefit exoplanet missions by substantially increasing system sensitivity, increasing mission lifetime, and lowering mission cost. We are developing a 256×256-pixel silicon focal plane array designed to have the features listed in the "Project Goal" column of Table 2, most notably zero read noise.

[‡] This level of signal quality is at the threshold to detect the presence of absorption bands of water, ozone, other molecules, vegetation, and oceans, which might be expected in spectra of terrestrial planets [27].

Ultimately, we anticipate raising the maturity of these detectors to TRL 6 on longer timescales by validating a prototype detector system in the JPL High Contrast Imaging Testbed [5]. Once the high-fill-factor 256×256 detectors are validated at TRL 6, we would seek to scale the design to megapixel arrays that satisfy the "Long-term Goals" column of Table 2. The architecture is scalable to larger formats, colder operation (for near- and mid-infrared applications), and smaller pixel size. The silicon detector technology is a pathfinder for developing InGaAs infrared versions that could use the same readout integrated circuits [6].

Table 2. Detector Performance

Parameter	*Project Goal*	*Long-term Goal*
Format	256×256	1024x1024
Pixel Size	25 µm	15 µm
Read Noise	zero	zero
Dark Current (@170 K)	<0.002 e^-/s/pixel	<0.001 e^-/s/pixel
Power[c] (mW)	<100	<250
QE[d] (350nm, 650nm, 1000nm)	50%,80%,30%	50%,80%,30%
Latent Image in 1000 seconds (after full well)	zero	zero
Fill Factor	100%	100%
Technology Readiness Level	5	6

[a]A 256×256 ROIC is in fabrication, but the hybridized device has 64×64 pixels.
[b]The 256×256 ROIC in fabrication has 25 µm pixels, but the hybridized device has 50 µm pixels.
[c]This quantity should be compared to detector+digitization electronics in other detectors.
[d]These values include the probability that photogenerated charges induce an avalanche.
[e]Requires lenslet array.

The approach for accomplishing the program is to fabricate, irradiate, and test photon-counting detectors in performance metrics relevant to *NASA* exoplanet missions. This work will advance the technology from TRL 3 toward TRL 5, following the criteria established in NASA NPR-7120.8 App. J [7]. In particular, it will demonstrate the performance of GM-APDs in the presence of a radiation environment that is representative of a typical exoplanet mission. We regard radiation effects as the most critical area of concern for this technology for advancement to TRL 5, although the technology must ultimately also pass testing in the presence of other environmental conditions, e.g. heat and vibration. The TPF-C Flight Baseline Mission Concept [8] defines exoplanet mission system characteristics for the purposes of this paper.

The detector design is described in detail in another paper [9]. Briefly, it uses an in-pixel triggering circuit that converts each absorbed photon into a relatively large voltage signal that can easily be detected by a CMOS readout circuit. The amplification is provided by a GM-APD that accelerates photogenerated charge in a region of high electric field. Each photodiode is connected to its own pixel circuit via a bump bond. The circuitry in each pixel registers the arrival of a photon and resets the photodiode so that it is ready to absorb another photon in ~100 ns.[§] A counter in each pixel accumulates photon absorption events. The readout circuit multiplexes the digital output of the counters for each pixel through output registers and digital buffers.

4. RADIATION TESTING

Radiation testing is the most important step in advancing GM-APD detectors to TRL 5. While other types of testing will also eventually need to be done, the technologies used in this program are directly derived from previous technologies that have successfully passed vibration and thermal testing, including those that have already flown in space. In particular, we will use the same legacy packaging techniques that have been used on all the NASA missions in which

[§] This is a relatively long time when considering the very low flux levels expected for an exoplanet mission. For instance, in spectroscopic mode, the flux is ~0.2 photons/s.

Lincoln Laboratory has supplied packaged detectors (ASCA, Chandra, Suzaku, EVE, etc.). The packaged GM-APDs will have the same NASA-qualified epoxies and bond wiring techniques. This includes bond pull testing of every bond wire to specification. The satellite-based package devices mentioned have been vibration, shock, and temperature tested to the specification of the stated missions.

The effects of radiation on the CMOS ROIC and GM-APDs will be determined by modeling and experiment, following a plan similar to that described in the European Space Agency's (ESA) handbook ECSS-E-HB-10-12 [10] and with guidance from JPL Publication 00-06 [11]. SPENVIS is used to determine the radiation environment on orbit. To determine the transported dose, a simple spherical shell of variable thickness is used to simulate the shielding around the APD in calculating the radiation dose, and an equivalent dose ten times higher than this will be used for radiation testing. The effects of radiation will be determined on the basis of ionizing and nonionizing radiation. Generally, the ionizing radiation effects scale with total ionizing dose (TID), while nonionizing radiation effects on such characteristics as dark-count rate scale with displacement damage dose (DDD) [12]. The DDD can be calculated by programs such as Shieldose, Mulassis, available in SPENVIS. The relative change in a property of interest can be determined in a given radiation environment by measuring the response to high-energy protons, 63 MeV for example, for a given TID and DDD, and scaling that response to that of the TID and DDD on orbit due to the integrated spectrum. This approach has worked well in space-qualifying several imagers for NASA missions (Chandra, ASCA, SUZAKU, HETE).

As an example, relating the change in dark current for a proton spectrum to the change in dark current (ΔI_D(spectrum)) for samples exposed to 63 MeV radiation (ΔI_D(63MeV)),

$$\frac{\Delta I_D(spectrum)}{\Delta I_D(63MeV)} = \frac{\int NIEL(E)\phi(E)dE}{NIEL(63MeV)\phi(63MeV)FWHM(63MeV)}, \qquad \text{Equation 1}$$

where NIEL(E) and ø(E) are the energy-dependent NIEL and flux of the proton spectrum (transported through any shielding) on orbit, NIEL(63MeV) and ø(63MeV) are the NIEL and flux used in the proton irradiation experiment on earth, and FWHM(63MeV) is the full-width half-maximum energy spread of the proton beam. The energy of 63 MeV has been used widely for testing CCDs since it is near the peak flux for several low-earth orbit spectra and it is the energy of the proton beam at the University of California, Davis, accelerator.

4.1 Radiation Effects

High-energy radiation affects focal plane detectors in a number of ways. These include increased dark current, threshold voltage drift, latch-up, and single-event upsets. Some of these effects are transient and can be completely mitigated through thermal annealing or even initiating a new exposure. Other effects contribute to cumulative degradation of performance during a mission lifetime. The short-term effect of this radiation is a slight degradation in signal-to-noise ratio. The long-term effects could be degradation in several categories. For a hybridized APD/CMOS focal plane, there are effects specific to each of the two components, the CMOS circuitry and the GM-APDs.

For the CMOS circuitry, ionizing radiation can produce single-event upsets that cause bit errors and, in the case of a bulk CMOS process, latch-up. It also produces damage that accumulates with dose. For CMOS circuits, this takes the form of charged defects in the gate and field oxides, which respectively shift transistor turn-on voltages and create parasitic leakage paths. Eventually, these effects can cause circuit malfunctions. One advantage of the Geiger-mode technology is that the CMOS pixel circuit is all digital, making it more robust than analog circuitry to total-dose effects.

Techniques for making the CMOS radiation hard are well known. They include circuit design and layout approaches, scaling to thinner gate oxides, and the use of silicon-on-insulator (SOI) CMOS technology. The photon-counting ROIC used in this effort was designed in a bulk 180 nm CMOS process under funding from another project. Radiation hardness was not a goal of the design, but we believe that there is a straightforward path to achieving it.

The principal concern in our effort is the radiation tolerance of the GM-APD based detectors. The APDs are inherently tolerant to single-event upsets, because even a large packet of charge produced by a high-energy particle or photon tends to trigger a single detection event. Nonionizing radiation, on the other hand, produces traps in the silicon that increase dark current, and therefore dark count rates, over time.

Previous measurements at Lincoln Laboratory have shown that a 24-µm pixel CCD has an increase in dark current of about 0.7 e^-/pix/s/(total rad) of 40 MeV protons at −20 °C. Fortuitously, the pixel area is close to that of a GM-APD

array of 25 μm cells, but the change in dark current due to radiation will scale with pixel area. Cooling will also reduce the dark current. The effect of temperature on dark count rate has been modeled as proportional to $e^{-\Delta E/kT}$, where ΔE is the activation energy, k is Boltzmann's constant, and T is the temperature. We have found that ΔE is greater than ~0.6 eV, half the energy gap of Si, indicating the dark count rate is typical of a well-behaved Si diode. Assuming a drop in temperature to −100 °C and exposure to 5 krad (Si) radiation at 40 MeV, we would expect an incremental increase in dark current of 0.005 e^-/pix/s compared to an unirradated detector at room temperature.

4.2 Radiation Environment

The total dose over the mission lifetime is dependent on the type of the mission orbit and on the relative phasing between the mission launch date and the solar cycle. It will also depend on the frequency and severity of solar storms during mission lifetime. To simulate the radiation environment faced by the focal plane, the radiation-testing program for this project considers two mission lifetimes of five and eleven years with a launch date of 2015. Most missions in Table 3 have nominal mission lengths of five years, and the eleven-year mission lifetime is considered to cover an entire solar cycle. Although the majority of proposed exoplanet missions would be located at L2, there are some missions with different orbits (see Table 3). As such, we consider four different types of orbits to determine the radiation environment faced by the focal plane [13], [14], [15], [16].

Table 3. List of potential future exoplanet missions.

Mission [17]		Location
SIM Lite		Earth-trailing heliocentric
Telescope for Habitable Exoplanets and Interstellar/Intergalactic Astronomy	THEIA	L2
New World Observer	NWO	L2
Terrestrial Planet Finder	TPF-C	L2
Extrasolar Planetary Imaging Coronagraph	EPIC	Earth-trailing heliocentric
Giant planets around M, L, T dwarfs in the Infrared	GIMLI	Earth-centered distant retrograde orbit (semimajor axis: 700,000 km)
Pupil-mapping Exoplanet Coronagraphic Observer	PECO	Heliocentric drift away orbit (like Kepler and Spitzer)
Transiting Exoplanet Survey Satellite	TESS	Low Earth Orbit (600km equatorial orbit)
Fourier-Kelvin Stellar Interferometer	FKSI	L2
PLAnetary Transits and Oscillations of stars	PLATO	L2
All Sky Transit Observer	ASTrO	L2
The Terrestrial and Habitable-zone Exoplanet Spectroscopy Infrared Spacecraft	THESIS	L2

SPENVIS is used to determine the expected radiation flux over the entire mission length at each orbit (see Figure 3). Low Earth Orbit (LEO) presents a very benign radiation environment at this particular alitutude (600 km) as the radiation flux there is far below those of the three other orbits. The solar protons are shielded by the geomagnetic field at LEO. Although the van Allen belt presents a harsh radiation environment, its relative contributions to the particle flux is relatively small for the other three orbits due to the short amount of time spent there. There is a significant flux of low energy trapped electron and protons, however, a moderate amount of shielding should stop these low energy particles. Solar protons, then, will be responsible for most of the ionizing and non-ionizing doses. The radiation flux at L2 is either comparable to or exceeds those of the other orbits. It is sufficient, therefore, to consider only the radiation flux on L2 orbit in determining radiation dose, especially given that most missions listed in Table 3 are located at L2.

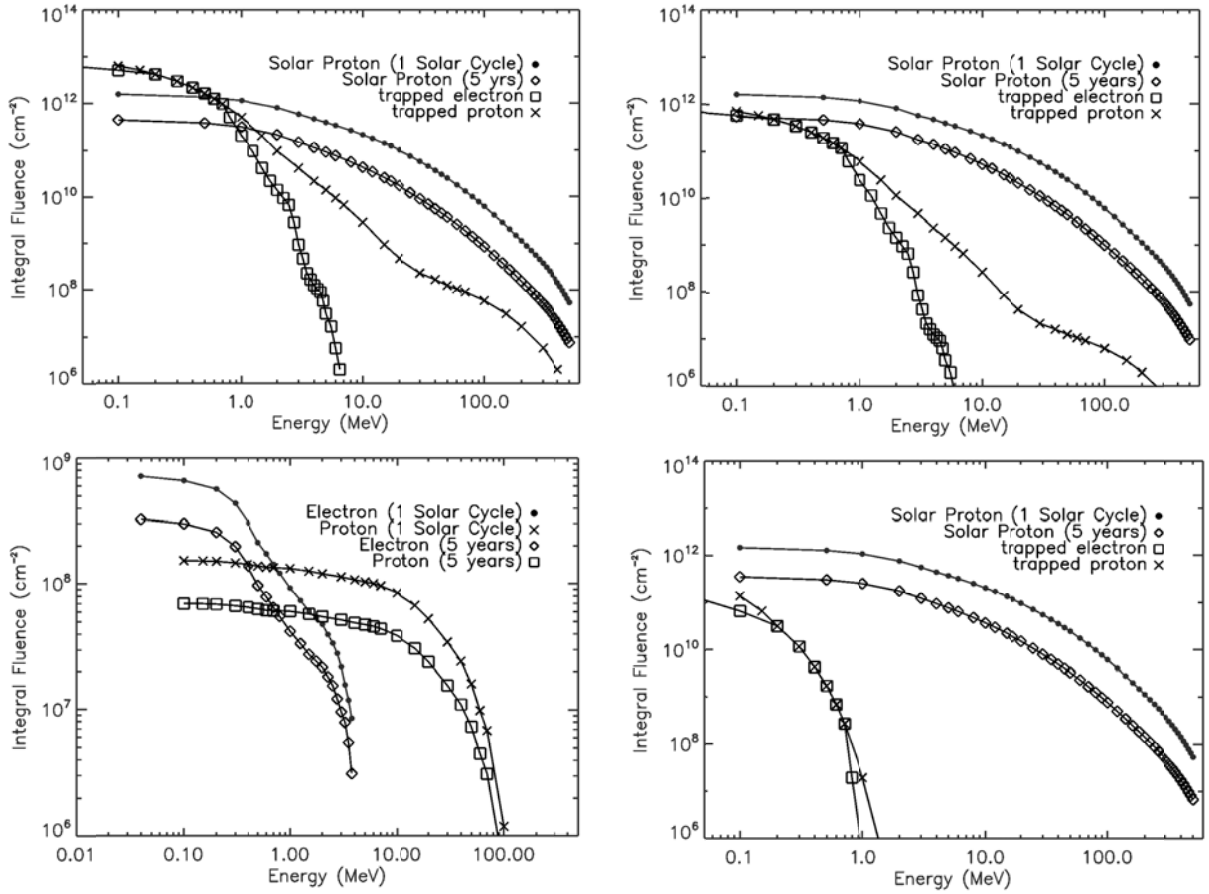

Figure 3. Integrated fluence, from indicated energy to infinity, versus particle energy at L2 (top left), distant retrograde orbit (top right), low earth orbit (bottom left), and earth-trailing heliocentric (bottom right), for mission durations of five (2015 launch date) and eleven years.

4.3 Radiation Test Program

The first step in designing a radiation testing program is to simulate the radiation field in the eventual operating environment, as described in Section 4.2. Second, the radiation field must be propagated through the spacecraft shielding which has the effect of attenuating particle energy and transmission. Third, the transported radiation must be translated into detector effects, the most severe of which have already been described above. Fourth, and finally, a ground-based test program must be devised to simulate the expected environment and radiation effects for a focal plane in space.

The radiation dose on the APD is estimated for a mission at L2 by taking the particle spectrum determined in Section 4.2 and simulating particle interactions with a simple spherical aluminum shielding and a silicon target. There are a number of particle transport simulation tools available both in SPENVIS and as standalone applications. Mulassis, a GEANT4-based simulation code available both in SPENVIS and as a standalone application, is used for this work [18], [19]. The results of simulation are shown in Figure 4. The protons and electrons trapped in the earth's radiation belts contribute a negligible amount to both the ionizing and non-ionizing radiation dose. Assuming a reasonable shielding thickness of ~10 mm, the total ionizing dose on the APD is ~1 krad and the displacement damage dose is ~2×10^7 MeV/g dose, for a 5 year mission at L2; for an 11 year mission, these numbers are 5 krad and 1×10^8 MeV/g, respectively. The radiation doses for a shielding thickness from 5 mm to 20 mm are within a factor 2 of those for the 10 mm case.

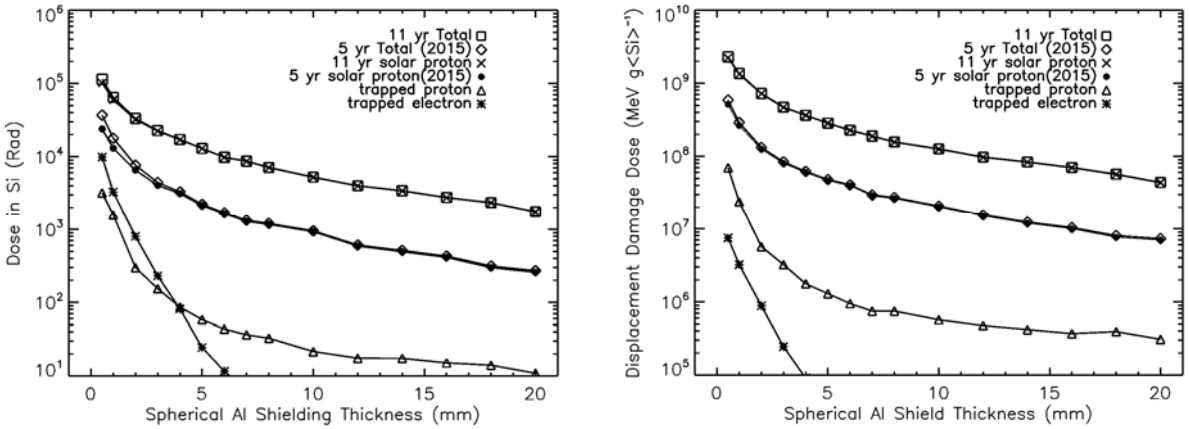

Figure 4. Cumulative total ionizing dose (left) and nonionizing dose (right) due to space radiation for a mission at L2 versus shield thickness, for spherically-shaped aluminum shielding. For a shield thickness of 10 mm, the total expected ionizing dose is approximately ~5 krad (Si) for a 11 year mission.

This last step, subjecting the APD to radiation at a radiation facility, requires significant interpretation because the wide spectrum of radiation, both in energy and species, encountered in space will normally exceed what is practically available on the ground, where it is often the case that monoenergetic high energy protons are the only radiation source used in testing. Also, the radiation dose rate during radiation testing will almost certainly far exceed the dose rate seen in space. As related above, radiation damage generally scales with radiation dose, and the expected radiation dose over the lifetime of the mission will be compared to the radiation dose that the APD is exposed to during radiation testing to predict the effects on the devices.

As radiation-induced dark current, a nonionizing radiation dependent quantity, is of primary concern for the APD, the proton is the appropriate choice for the particle species for radiation testing. Almost the entire displacement damage dose is due to protons (see Figure 4). Figure 5 shows, for example, the solar proton spectrum transported through 13 mm of aluminum shielding and the NIEL weighted spectrum, obtained by convolving the NIEL for protons in silicon with the said post-shielding solar proton spectrum. The solar proton spectrum transported through the shielding has a mean around 70 MeV, while the NIEL weighted spectrum has a mean around 50 MeV. These quantities are, of course, dependent on the thickness of the shielding, but for a range of thickness from 5 to 17 mm, the means are between 40 and 70 MeV. This means, roughly speaking, an equal amount of DDD is contributed by particles above and below 60 MeV, and there is an equal number of particles above and below 60 MeV. Also, 60 MeV happens to be where the ratio between the TID and DDD at L2 is preserved. For example, 3.5×10^{10} protons at 60 MeV subjects silicon to an exposure of 5 krad TID and 1×10^{8} MeV/g (DDD), which are very close to the radiation doses seen by the APD for an 11-year mission at L2 (see Figure 4). 60 MeV proton is, therefore, a good choice to simulate the radiation effects on the APD. The APD will be exposed to a final dose of 50 krad TID, or about 10 times the dose for an 11-year mission. This large safety margin should mitigate any deficiencies arising from assumptions such as the use of simple shielding geometry and simulate the viability of the APD for the worst-case scenario in the space radiation environment.

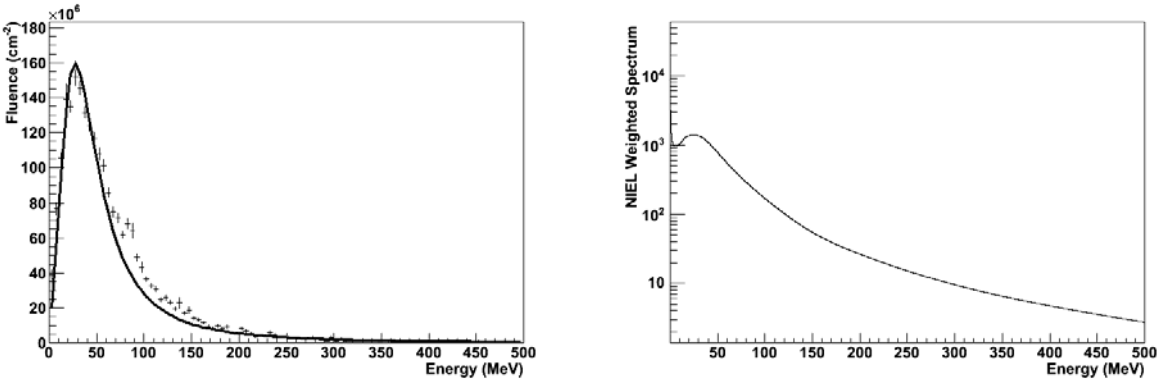

Figure 5. Solar proton spectrum transported through 13 mm aluminum shielding, which follows the Landau distribution closely (left), and NIEL weighted solar proton spectrum (right).

5. DETECTOR PERFORMANCE CHARACTERISTICS DEFINITIONS

A key challenge for an exoplanet mission is to detect a planet that contributes a very faint flux. Potential noise sources for both spectroscopy and imaging are read noise, shot noise from the residual light from the star, shot noise from the zodiacal light, and shot noise from dark current. The following are the most relevant detector performance characteristics in the context of an exoplanet mission.

5.1 Read Noise

Read noise is the uncertainty in the estimated signal value produced by a detector exposed to no light and having negligible dark events per exposure. It is defined to be an intrinsic property of the light-sensitive structure and the readout circuit. It does not include shot noise from any source or noise in downstream electrical components, e.g. cables, amplifiers, and analog-to-digital converters.

5.2 Dark Count Rate

Dark count rate is the rate of events generated at the readout circuit output while the detector is in complete darkness. Note that this can differ from dark current, some fraction of which might not generate events; this is the case for dark charge that is not amplified enough to trigger the event discriminating circuitry in the readout circuit.

5.3 Intrapixel response

Intrapixel response describes the uniformity of response across the full area of the pixel.

5.4 Quantum Efficiency

Quantum efficiency is the ratio of detected events to incident photons. It is the product of several probabilities: transmission, absorption, diffusion, amplification, and triggering.

5.5 Afterpulsing

Afterpulsing describes the tendency of an individual APD pixel to produce a burst of events after an avalanche has been initiated and quenched in that pixel. An afterpulse can be triggered when charge produced in the original avalanche becomes trapped in material defect sites and later migrates from the trap to the high field region. It can also be produced if charge from the original avalanche is temporarily stored in the absorber region while the depletion region is debiased. Afterpulsing is a function of avalanche time, quench time, pixel geometry, field geometry, biasing, and the trap population.

5.6 Persistent Charge

Persistent charge is the charge that becomes trapped in the light-sensitive portion of the detector and then becomes liberated and counted as events in later exposures.

5.7 Dynamic Range

Dynamic range is the ratio of the maximum to minimum signal.

5.8 Radiation Exposure in a Relevant Environment

Radiation exposure in a relevant environment describes exposure of a device to radiation flux, fluence, energy distribution, and particle distribution that mimics the expected exposure in a mission design.

5.9 Crosstalk

Crosstalk generates events in one pixel as a result of activity in another pixel or output channel. It can be induced by electrical interference, charge diffusion or photon generation during charge avalanche. For the architecture used in this project, the output signals are converted to digital form in the pixel circuit, so electrical crosstalk that normally affects weak analog signals in most detectors will not be important. Charge diffusion is as much a concern in the current architecture as it is for any detector. Optical crosstalk is potentially more of a discriminator for comparing the current architecture to that of typical detectors. This is because the photoexcitation of nearby pixels depends on photoemission in the avalanche process.

5.10 Estimating Rates

The measured event rates will be less than the true rates due to detector dead time. There are two types of dead time in the system. One is due to the APD quench/reset time; this is on the order of 100 ns. The other is due to the nature of the Geiger mode operation. The APD can detect at most one event per cycle. Once an avalanche has been initiated, the pixel cannot detect another event until the pixel is re-armed. In this sense, the pixel is "dead" to new photons for the rest of the cycle. Figure 6 shows a time sequence of the relevant events.

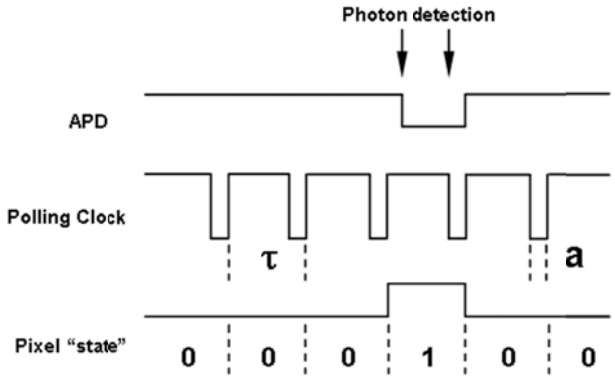

Figure 6. Clock diagram showing the timing relationship between photogenerated events and system state. Note that the same relationships hold for dark current generated events.

The counted events can be used to estimate the number of events that would have been counted in the absence of dead time. The trigger probability during one cycle is given by the Poisson probability of getting at least one event during that cycle. Summed over all cycles, the mathematical relationship between the two is given in Equation 2.

$$\bar{c} = N \times (1 - e^{-\rho\tau}), \qquad \text{Equation 2}$$

where $\bar{c}$ is the counted events, N is the number of cycle times, ρ is the expected rate in the absence of dead time and τ is the cycle time. From Equation 2, it is apparent that in the limit of low flux, measured counts will be linearly proportional to ρτ. This is due to the fact that the probability of more than one photon arriving during one cycle is negligible. In the upper limit, the measured counts will asymptotically reach the number of cycles, i.e. the APD is triggered every cycle. These behaviors can be seen in the real device [9]. The variance, $\bar{\sigma}_c^2$, is given in Equation 3.

$$\overline{\sigma}_c^2 = N(1-e^{-\rho\tau})e^{-\rho\tau}. \qquad \text{Equation 3}$$

For the purposes of this project, results will be reported in both counted events and inferred expected number of events. For best results, we will attempt to obtain data in regimes where this correction is not important, i.e. the fluxes are low. This formulation, and strategy, is valid both for photo-induced events and multiplied dark current-induced events.

6. THE PATH TO SPACE QUALIFICATION

GM-APD array detectors are at TRL 3, "Analytical and experimental critical function and/or characteristic proof-of concept." There are several capabilities of these detectors for which "critical function" has been established. These include: 1) single photon event triggering, 2) active avalanche quenching, and 3) triggering and re-arming. The most critical capability of these detectors for the exoplanet application is single photon detection and counting. These functions have been validated and patented [20], [21], [22], [23], [24], [25].

This project will validate a photon-counting imager ("component") in a "laboratory environment" (=TRL 4) and in a simulated mission-like "relevant environment" that includes exposure to high-energy radiation, in partial fulfillment of the requirements for TRL 5. Note that as part of the technology advancement, the measured performance will be compared to that predicted by analytical models and competing technologies, e.g. EMCCDs. This process includes the definition of such analytical models at the earlier TRLs. During the current activity, a relevant sensitivity metric will be developed. One likely candidate for such a metric is SNR versus fluence normalized to an ideal detector (c.f. Figures 4 and 10 in [26]).

ACKNOWLEDGEMENTS

This project was funded by the NASA Technology Demonstration for Exoplanet Missions (TDEM) program under grant NNX10AF82G.

REFERENCES

[1] [Online]. http://planetquest.jpl.nasa.gov/

[2] "TPF-C Flight Baseline Mission Concept Report,". [Online]. http://planetquest.jpl.nasa.gov/TPF-C/TPFC-MissionAstro2010RFI-Final-2009-04-01.pdf

[3] "TPF-C STDT Report,". [Online]. http://planetquest.jpl.nasa.gov/TPF/STDT_Report_Final_Ex2FF86A.pdf

[4] J T Trauger and W A Traub, "A laboratory demonstration of the capability to image an Earth-like extrasolar planet," *Nature*, vol. 446, p. 771, 2007.

[5] [Online]. http://exep.jpl.nasa.gov/documents/4-ExEP-C_Infrastructure_s.pdf

[6] [Online]. ttp://www.rle.mit.edu/llseminar/documents/Flyer_Verghese10-8.pdf

[7] "NPR-7120.8 App. J.,". [Online]. http://nodis3.gsfc.nasa.gov/displayDir.cfm?Internal_ID=N_PR_7120_0008_&page_name=AppendixJ

[8] M Levine, D Lisman, and S Shaklan, "TPF-C Flight Baseline Mission Concept," JPL, 2009. [Online]. http://planetquest.jpl.nasa.gov/TPF-C/TPFC-MissionAstro2010RFI-Final-2009-04-01.pdf

[9] D F Figer et al., "Silicon single photon imaging detectors," in *SPIE*, vol. 8155B, Bellingham, 2011.

[10] "Standards for Space Radiation Environments and Effects," European Space Agency's (ESA) handbook ECSS-E-HB-10-12. [Online]. https://escies.org/GetFile?rsrcid=307

[11] "An Introduction to Space Radiation Effects on Microelectronics," JPL, JPL Publication 00-06 2000. [Online]. http://parts.jpl.nasa.gov/docs/JPL00-62.pdf

[12] J R Srour and D H Lo, "Universal Damage Factor for Radiation-Induced Dark Current in Silicon Devices," *IEEE Transactions on Nuclear Science*, vol. 47, no. 6, pp. 2451-2459, 2000.

[13] wmap. [Online]. http://lambda.gsfc.nasa.gov/product/map/dr1/pub_papers/firstyear/supplement/WMAP_supplement.pdf

[14] gimli. [Online]. http://exep.jpl.nasa.gov/presentations/76-GIMLI_2009final.pdf

[15] sirtf. [Online]. http://kepler.nasa.gov/Mission/QuickGuide/MissionDesign/launchVehicleAndOrbit/

[16] leo. [Online]. http://nexsci.caltech.edu/workshop/2007/Latham.pdf

[17] (2008) EXOPLANET FORUM 2008. [Online]. http://exep.jpl.nasa.gov/exep_exfPresentations.cfm

[18] J Allison, K Amako, J Apostolakis, H Araujo, and P Arce Dubois, "Geant4 developments and applications," *IEEE Transactions on Nuclear Science*, vol. 53, no. 1, pp. 270-278, 2006.

[19] F Lei et al., "MULASSIS: A Geant4-Based Multilayered Shielding Simulation Tool," *IEEE Transactions on Nuclear Science*, vol. 49, no. 6, pp. 2788-2793, 2002.

[20] S. Cova, M. Ghioni, A. Lacaita, and F. Zappa, "Avalanche photodiodes and quenching circuits for single-photon detection," *Applied Optics*, vol. 35, pp. 1956-1976, 1996.

[21] M A Albota et al., "Three-dimensional imaging laser radar with a photon-counting avalanche photodiode array and microchip laser," *Appl Opt.*, vol. 41, no. 36, pp. 7671-8, Dec 2002.

[22] R M Marino et al., "A compact 3D imaging laser radar system using Geiger-mode APD arrays: system and measurements," *SPIE*, vol. 5086, pp. 1-15, 2003.

[23] B F Aull, "3D Imaging with Geiger-mode Avalanche Photodiodes," *Optics and Photonics News*, vol. 16, pp. 42-46, 2005.

[24] B Aull et al., "Laser radar imager based on three-dimensional integration of Geiger-mode avalanche photodiodes with two SOI timing-circuit layers," *ISSCC Dig. Tech. Papers*, pp. 304-305, 2006.

[25] Cristiano Niclass and Edoardo Charbon, "Integrated circuit comprising an array of single photon avalanche diodes," 11353244, 2009.

[26] O Daigle et al., "CCCP: a CCD controller for counting photons," *SPIE*, vol. 7014, pp. 70146L-70146L-10, 2008.

[27] N J Woolf, P S Smith, W A Traub, and K W Jucks, "The Spectrum of Earthshine: A Pale Blue Dot Observed from the Ground," *ApJ*, vol. 574, p. 43, 2002.